Neutron Spectroscopy in Perpendicular Neutral Beam Injection Deuterium Plasmas Using Newly Developed Compact Neutron Emission Spectrometers

Exploration of Helically-Trapped Fast Ion Behavior in Deuterium Plasmas Using Newly Developed Perpendicular Compact Neutron Emission Spectrometers

Siriyaporn Sangaroon, Kunihiro Ogawa, Mitsutaka Isobe, Longyong Liao, Guoqiang Zhong, Apiwat Wisitsorasak, Eiji Takada, Makoto Inami Kobayashi, Nopporn Poolyarat, Sadayoshi Murakami, Ryohsuke Seki, Hideo nuga, and Masaki Osakabe

***Abstract*—The presence of helically-trapped fast ions in helical ripple in Large Helical Device (LHD), resulting from perpendicularly injected positive-ion-source-based neutral beam (P-NB) heated plasma and/or from ion cyclotron range of frequency (ICRF) wave heated plasma, poses a significant concern due to the system's lack of symmetry. In response to this challenge, compact neutron emission spectrometers (CNESs) have been strategically developed in the LHD, featuring a perpendicular field of view relative to the plasma's magnetic field. The first perpendicular CNES offers a vertical field of view through the deuterium plasma and incorporates a liquid (EJ-301) scintillation detector optimized for efficient operation across a broad range of neutron emission rates. The second perpendicular CNES is constructed using a Cs_2LiYCl_6:Ce scintillation detector enriched with ^{7}Li (CLYC7), providing a horizontal field of view through the deuterium plasma and effectively operating in a region characterized by relatively low neutron emission rates. During plasma heating through P-NB, both perpendicular CNESs showcase a distinctive neutron energy distribution, featuring a double-humped profile with two peaks at energy of approximately 2.30 MeV and 2.74 MeV. Furthermore, we utilized the DELTA5D code for orbit-following in five dimensions to ascertain the expected spectrum of neutron energy distribution. Notably, the calculated neutron energy spectrum arising from the deuterium-deuterium reaction closely mirrors the experimental results, affirming the accuracy and reliability of using perpendicular CNES for investigating the dynamics of fast ions helically trapped in the LHD. These peaks align with the Larmor motion of deuterons resulting from P-NB injection at the helical ripple of the LHD. Additionally, we conducted neutron spectrometry involving deuterium-deuterium interactions in a deuterium plasma simultaneously heated by both P-NB and ICRF waves, characterized by a high neutron emission rate, utilizing perpendicular CNES based on EJ-301. The observation revealed an expansion in spectrum width, attributed to the additional ICRF wave heating.**

***Index Terms*—Large Helical Device, NB injection, ICRF wave, Compact neutron emission spectrometer, EJ-301, CLYC7.**

Manuscript received XX; revised XX; accepted XX. Date of publication XX; date of current version XX. This study received partial support from NIFS Collaboration Research Programs (KOAH037) and the NINS program for Promoting Research by Networking among Institutions (Grant Number 01411702). Additionally, funding was provided through the Japan-China Post-Core-University-Program known as Post-CUP, the Excellence Program of Hefei Science Center CAS (No.2020HSC-UE012), and Thailand Science Research and Innovation (TSRI) via the Fundamental Fund FY2566 (Contract Number 2589646/4369740). SS acknowledges financial support from the Program Management Unit for Human Resources and Institutional Development, Research and Innovation, PMU-B fiscal year 2023 (Grant No. B37G660016).

Siriyaporn Sangaroon is with the Department of Physics, Faculty of Science, Mahasarakham University, Maha Sarakham 44150, Thailand (e-mail:siriyaporn.s@msu.ac.th).

Kunihiro Ogawa, Mitsutaka Isobe, Makoto Inami Kobayashi, Ryohsuke Seki, Hideo nuga and Masaki Osakabe are with the National Institute for Fusion Science, Toki 509-5202, Japan, and also with the Department of Research, Graduate University for Advanced Studies, SOKENDAI, Hayama 509-5202, Japan (e-mail:ogawa.kunihiro@nifs.ac.jp; isobe.mitsutaka@nifs.ac.jp; kobayashi.makoto@nifs.ac.jp; seki.ryohsuke@nifs.ac.jp; nuga.hideo@nifs.ac.jp; osakabe.masaki@nifs.ac.jp).

Longyong Liao is with the Department of Research, Graduate University for Advanced Studies, SOKENDAI, Hayama 509-5202, Japan (e-mail:liao.longyong@nifs.ac.jp).

Guoqiang Zhong is with the Institute of Plasma Physics, Chinese Academy of Sciences, Hefei 230031, China (e-mail:gqzhong@ipp.ac.cn).

Apiwat Wisitsorasak is with the Department of Physics, Faculty of Science, King Mongkut's University of Technology Thonburi, Bangkok 10140, Thailand (e-mail:apiwat.wis@mail.kmutt.ac.th).

Eiji Takada is with the National Institute of Technology, Chiyoda 101-0003, Japan (e-mail:e_takada@kosen-k.go.jp).

Nopporn Poolyarat is with the Thailand Institute of Nuclear Technology, Bangkok 10900, Thailand (e-mail:nopporn@tint.or.th).

Sadayoshi Murakami is with the Department of Nuclear Engineering, Kyoto University, Nishikyo, Kyoto 615-8540, Japan. (e-mail:murakami.sadayoshi.7a@kyoto-u.ac.jp).

Digital Object Identifier XX

I. Introduction

In nuclear fusion devices, plasmas are primarily heated by neutral beam (NB) injection and by ion cyclotron range of frequency (ICRF) waves, serving as a primary sources of fast ions. Comprehending fast ion transport is a crucial aspect for achieving fusion plasma with the high performance and paving the approach to a fusion reactor [1]. The occurrence arises due to the self-sustaining state of the fusion reactor is sustained through the self-heating mechanism propelled by fast ions generated in the fusion process, specifically alpha particles of 3.5 MeV produced in D(T,n)α reaction. Simultaneously, comprehending fast ion transport resulting from magnetohydrodynamic (MHD) instability induced by fast ions is a key focus in research on fast ion confinement [2]. The exploration of confined fast ion behavior in the fusion plasma has been successfully demonstrated using various fast ion diagnostics [3]. The most common diagnostics for the study of fast ion confinement are fast-ion D-alpha spectroscopy (FIDA) [4], [5] and neutral particle analyzers (NPA) [6], [7]. These diagnostic techniques involve active measurements, necessitating the injection of a beam and subsequent measurement of signals, which depend on plasma parameters and

the beam injection. In contrast to FIDA and NPA, fast ion confinement has been successfully demonstrated by utilizing emitted neutrons through neutron emission spectrometry (NES) [8]. This approach is based on the recognition that the physics associated with fast ions is evident in neutron emissions resulting from fusion reactions, such as D(D,n)^{3}He reaction and D(T,n)α reaction [9], [10], [11]. NES systems incorporate techniques such as time-of-flight proton recoil [12] and time-of-flight methods [13]. Furthermore, the utilization of a compact neutron emission spectrometer (CNES) provides a distinct advantage in examining fast ion distributions in both real and phase spaces. The standard detectors used in CNES include diamond detectors [14], [15] and liquid scintillators [16], [17].

In the setting of the Large Helical Device (LHD), a study on the transport of fast ions caused by MHD instabilities driven by fast ions in the NB heated plasma has been conducted [18]. In hydrogen plasma experiments, the retention of fast ions produced through NB injection and ICRF wave heating was investigated [19], utilizing an extensive set of fast ion diagnostic tools [20]. Specifically, the study focused on the confinement characteristics of helically-trapped protons accelerated through ion cyclotron resonance heated plasma. This investigation utilized NPA based on diamond detectors [21]. The investigation of fast ions transport and loss associated with toroidal Alfvén eigenmode has been performed utilizing a NPA [22] and a detector specifically designed for observing fast ion loss [23]. While the comparison of experimental results and numerical simulations has unveiled insights into the fast ion transport and fast ion loss processes induced by toroidal Alfvén eigenmode [24], [25], the information accessible regarding fast-ion confinement has been restricted in both real and phase spaces. Initiating the deuterium plasma experiment in LHD in March 2017 facilitated the study on confined fast ions through neutron measurements. The LHD incorporates three tangentially injected neutral beam injections (N-NBs) utilizing negative-ion sources and two perpendicularly injected neutral beam injections (P-NBs) utilizing positive-ion sources. These systems collectively provide heating power of up to 35 MW. Neutron are produced through fusion reactions, specifically D(D,n)^{3}He, occurring between fast ions generated by NB and bulk ions. Neutron measurements offer direct insights into the dynamics of fast ions within the plasma core. The maximum value of total neutron emission rate (S_n) in LHD is estimated to reach 1.9 $\times$ 10^{16} n/s [26]. Consequently, comprehensive neutron diagnostics have been established at LHD to deepen the comprehension of fast-ion physics [27], [28], [29], [30]. The dynamics of fast ions helically confined following P-NB injections plays a crucial role in comprehending core plasma physics. This significance is especially emphasized due to the lack of symmetry in LHD, which can lead to challenges in fast ion loss and the limitation of ion temperature. Starting from 2018, highly efficient vertical neutron cameras (VNC) have been designed for use on the LHD. These VNCs are designed to measure neutron emission profiles, enabling the visualization of poloidal structures associated with helically-trapped fast ions produced by P-NB heating [31], [32]. Extensive investigations employing the VNC have been conducted to analyze the transport and loss of fast ions caused by helically-trapped fast ions in the LHD [33], [34], [35]. Even though the behavior of fast ions has been intensively studied in the LHD, measurements in real and phase spaces are still lacking. To observe the behavior in real and phase spaces in the LHD, neutron spectroscopy has been effectively facilitated by the NES system, specifically the time-of-flight enhanced diagnostics (TOFED) [36], [37] and CNES [38], [39], [40], [41]. To improve the understanding of the behavior of helically-trapped fast ions during P-NB heating, perpendicular CNES systems with a sight-line oriented perpendicular to the magnetic field, operating across a broad range of S_n, have been employed. This paper explores neutron emission measurements from deuterium-deuterium reactions during plasma heating with P-NB, utilizing newly developed perpendicular CNESs in the LHD. The structure of the paper is as follows: Section II present neutron emission patterns reflecting fast ions in fusion plasma. Section III provides detailed information about the perpendicular CNESs. The numerical simulation of the neutron spectrum anticipated for measurement by these perpendicular CNES systems, is described in Section IV. In Section V, the results of neutron emission spectrometry from deuterium-deuterium reactions in plasmas undergoing P-NB heating are presented. To conclude, Section VI provides a summary of this work.

II. Patterns of neutron emission that reflect the fast ion's behavior in the LHD

The LHD stands as the world's largest stellarator/helical system, providing the ability for continuous operation and a system free from disruptions. It is situated at the National Institute for Fusion Science (NIFS) in Gifu, Japan. A crucial focus of research at LHD involves gaining a deeper understanding of fast ion physics and confinement properties. This emphasis is particularly noteworthy since the predominant fraction of fast ions is anticipated to consist of alpha particles originating from deuterium-tritium plasma, a vital consideration for future fusion reactors. In Fig. 1a, a schematic top-view perspective of the LHD is presented, showcasing the locations of N-NBs and P-NBs injections, along with the perpendicular CNESs situated at the 1.5-L lower port and 8-O horizontal port. Note that N-NB#1 and N-NB#3 deliver fast ion circulating in counter clockwise direction while N-NB#2 delivers fast ion circulating in clockwise direction. P-NB#4 and P-NB#5 deliver fast ions perpendicular to the helical ripple of the LHD. The tangential injection N-NBs provide a high-energy fast ions at approximately 190 keV, whereas the perpendicular injection P-NBs deliver fast ions with an energy level of around 80 keV. Fig. 1b illustrates a poloidal cross-section elongated in the horizontal direction, depicting the injection of P-NB at the helical ripple. The Poincaré plot of the orbit of helically-trapped fast ions generated by the P-NB was calculated. The computation was executed utilizing the collisionless Lorentz orbit code known as LORBIT [42], setting the fast ion energy of the beam ion to 80 keV. These fast ions were injected perpendicularly to the magnetic field, and the initial pitch angle could occur within a range of 89 degrees which the ion become trapped within the helical ripple.

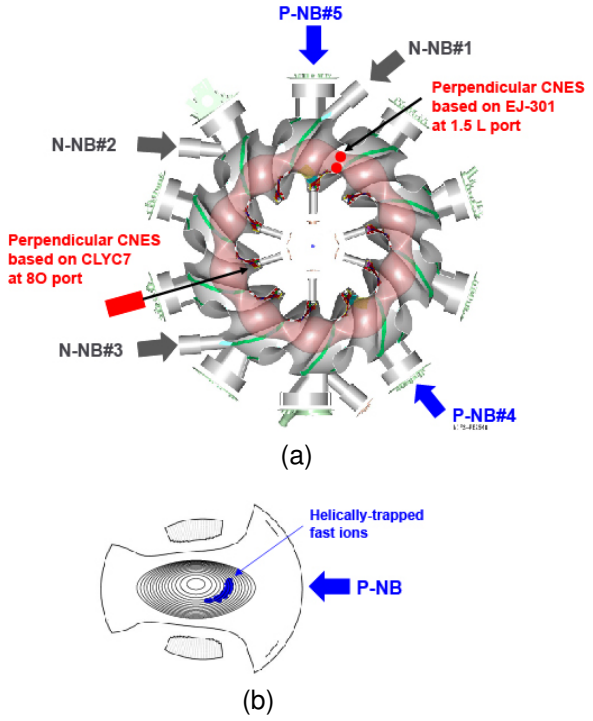

Fig. 1. (a) A schematic top-view of the LHD, showing the positions of P-NB injections. A perpendicular CNES based on EJ-301 was placed at radii (R) of 3.725 m and 3.875 m at the 1.5-L port, while a perpendicular CNES based on CLYC7 was installed at the 8-O port. (b) The Poincaré plot depicts the trajectory of helically-trapped fast ions with a pitch angle of 89 degrees.

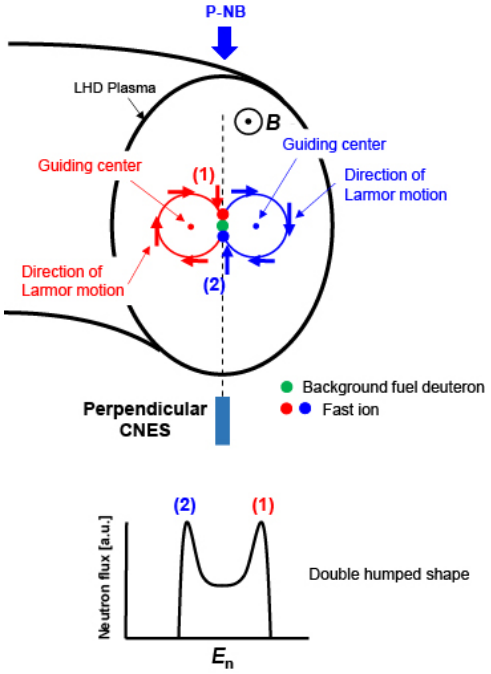

Fig. 2. Expected observations of the energy distribution of neutrons resulting from deuterium-deuterium interactions in P-NB heated plasma as measured by the perpendicular CNES.

After the fusion reaction between the fast ion (fast deuteron) injected by the NB and the background fuel deuteron, neutrons are generated. The neutron energy, denoted as E_n, can be formulated within the center-of-mass frame as: [43]:

$$E_n = \frac{1}{2} m_n v_{COM}^2 + \frac{m_{He_3}}{m_{He_3} + m_n}(Q_{DD} + K) + v_{COM} cos(\theta) \sqrt{\frac{2 m_{He_3} m_n}{m_{He_3} + m_n}(Q_{DD} + K)} \quad (1)$$

where K equal to $1/2\mu v_{rel}^2$. v_{COM} equal to $(m_{D1}v_{D1} + m_{D2}v_{D2})/(m_{D1} + m_{D2})$. m_n is mass of neutron, m_{He_3} is mass of ^3He, m_{D1} is mass of fast deuteron, m_{D2} is mass of background fuel deuteron, v_{COM} is center-of-mass velocity of the reaction, v_{rel} is relative velocity, Q_{DD}, equal to 3.27 MeV, stands for the overall energy release resulting from the D(D,n)^{3}He reaction. In this context, K denotes the relative kinetic energy between fast deuteron and background fuel deuteron, μ signifies the reduced mass of deuterons, and v_{D1} represents the relative velocities of the fast deuteron. v_{D2} signifies the relative velocities of the background fuel deuteron, v_n corresponds to the neutron velocity, and θ represents the angle between v_{COM} and v_n. In the context of a thermal deuterium-deuterium plasma, the energy spectrum E_n displays a nearly Gaussian distribution, centered around 2.45 MeV. However, in plasma heated by NB, where $v_{D1} \gg v_{D2}$, the neutron energy spectrum experiences a Doppler shift. In this scenario, it can be asserted that when v_{COM} aligns with v_n (θ = 0°), E_n will achieve its peak, indicating an upward shift in the energy of deuterium-deuterium neutrons. Conversely, if v_{COM} is opposite to v_n (θ = 180°), E_n will reach its minimum energy, indicating a reduced shift in the energy of deuterium-deuterium neutrons. If v_{COM} is orthogonal to v_n (θ = 90°), the alteration in deuterium-deuterium neutron energy becomes negligible. In the LHD, in high-energy tangential injection N-NB heating plasma, a Doppler shift occurs in the context of the neutron energy spectrum when the velocity of the fast deuteron surpasses that of the background bulk ions. This phenomenon has been effectively observed utilizing tangential CNESs [39], [44], [38]. In the scenario of N-NB#1 and N-NB#3 heated plasma, the neutron energy spectrum from deuterium-deuterium reactions reveals a peak at a higher energy, corresponding to the v_{COM} of the circulating deuterium-deuterium reaction directed toward the tangential CNES. Conversely, under N-NB#2 heating, the spectrum shows a peak at a lower energy level, corresponding to the v_{COM} of the deuterium-deuterium reaction moving away from the tangential CNES. As anticipated, during P-NB heating, the neutron energy spectrum for deuterium-deuterium reactions exhibits a peak at approximately 2.45 MeV, aligning with the velocity of the reactants moving perpendicular to the sight-line of the tangential CNES.

In P-NB heating, when fast ions are injected into helical ripple of the LHD with a pitch angle near 90 degrees, these ions become trapped within the ripple. The resulting $v_\perp \gg V_\parallel$ condition further ensures that fast ions are effectively confined within the ripple. Fig. 2 depicts the behavior of a fast ion and background fuel deuteron during P-NB heating, illustrating its rotation orthogonal to the magnetic field (represented as a dot). In the fusion reaction, deuterium-deuterium neutrons are generated. In this study, the measurement of deuterium-

deuterium neutrons during P-NB heating will be conducted using neutron spectroscopy, specifically the perpendicular CNESs positioned at the LHD helical ripple location, with the sight-line oriented perpendicular to the magnetic field. When v_{COM} of the reaction is moving downward along the line-of-sight, v_{COM} aligns with v_n (θ = 0°), an increase in energy of neutron denoted as (1) is anticipated. Conversely, when v_{COM} is moving upward along the line-of-sight, v_{COM} is opposite to v_n (θ = 180°), a decrease in energy of neutron denoted as (2) is expected. The neutron energy spectrum resulting from deuterium-deuterium reaction, characterized by the double-humped structure, corresponding to the Larmor motion of deuterons from P-NB heating, is anticipated to be detected by the perpendicular CNES.

III. Perpendicular Compact Neutron Emission Spectrometers

To enhance our comprehension of the dynamics of fast ions helically confined in P-NB heated plasma and the acceleration of fast ions induced by ICRF waves in the LHD, we employed perpendicular CNESs with a line-of-sight oriented perpendicular to the magnetic field. These setups incorporate a traditional liquid (EJ-301) scintillation detector and a newly designed Cs_2LiYCl_6:Ce scintillation detector enriched with ^{7}Li (CLYC7).

A. Perpendicular CNES based on EJ-301

A perpendicular CNES based on EJ-301 was employed since 2021 [45]. Conventional EJ-301 scintillation detector was chosen for perpendicular CNES due to their effective pulse shape discrimination (PSD) capabilities, high neutron detection efficiency, and ability to provide a fast decay time signal. Two vertically-oriented line-of-sight perpendicular CNESs were installed at the 1.5-L lower port of the LHD [see Fig. 3]. These perpendicular CNESs were configured to provide a poloidal view of the plasma. The detectors were accurately placed at radial distances (R) equal to 3.725 m and 3.875 m, and they were aligned with concrete collimators, 150 cm in length with a 5 cm diameter. These perpendicular CNESs were positioned 7 m at a distance from the plasma mid-plane. The results presented in this paper originated from the perpendicular CNES positioned at R equal to 3.725 m. The EJ-301 scintillator employed in these perpendicular CNES units had dimensions of 2.54 cm in diameter and height [46]. It was paired with photo-multiplier tubes (PMTs) with a diameter of 2.54 cm, specifically model H10580-100-01 of Hamamatsu Photonics K.K. [47]. To apply a high voltage of -1000 V to the detector, we employed a quad high-voltage power supply, specifically model RPH-033 of HAYASHI-REPIC Corp. [48]. For data acquisition, we utilized a high-speed digital data acquisition system, model APV8102-14MWPSAGb of Techno AP Corp. [49]. Signals were transmitted through a 1 Gbps Ethernet connection and then archived in the LHD experiment database.

The neutron-induced signal in the EJ-301 scintillation detector exhibits a fast decay time, typically on the order of nanoseconds. As a result, the perpendicular CNES based on

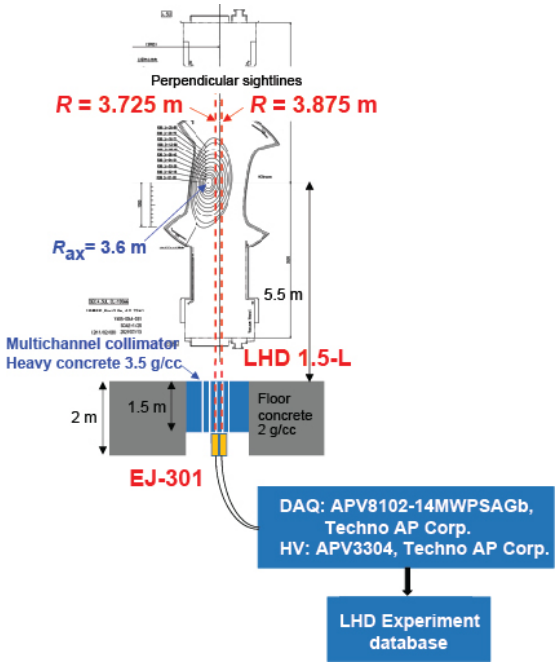

Fig. 3. A schematic cut view of the LHD, showing the vertical line-of-sight perpendicular CNES based on EJ-301 operating at the LHD 1.5-L port.

EJ-301 demonstrates the capability to measure a broad range, extending up to the maximum value of S_n [44]. Nevertheless, the measurement of deuterium-deuterium neutrons using EJ-301 scintillation detector involves detecting the recoiled proton created by elastic collisions, necessitating spectrum unfolding. We employed the derivative unfolding technique [50] to extract the spectrum energy of neutron from its recoil proton, as measured by perpendicular CNES [39], [44], [45]. This method relies on the established correlation between recoil proton energy (E_p) and light output (L) [51]. The unfolded neutron spectrum was derived by computing the differential neutron flux ($\phi(E_n)$), represented as [50]:

$$\phi(E_n) = \frac{-E_p}{TnV\sigma(E_p)}[y'(x)\{gL'(E_p)\}^2 + y(x)gL''(E_p)] \tag{2}$$

here, T signifies the duration of time [s], n denotes the hydrogen atom density [cm^3], V represents the volume of sensitivity [cm^3], $\sigma(E_p)$ stands for the cross-section for neutron-proton elastic scattering as a function of E_p [cm^2], $y(x)$ illustrates the Q_{total} histogram, and g is the PMT's gain, set at 6.6×10^5. Note that $'$ indicates the first derivative and $''$ indicates the second derivative. In this study, the efficiency of the detector was not considered.

B. Perpendicular CNES based on CLYC7

The second perpendicular CNES was built upon a recently developed CLYC7 scintillation detector because CLYC7 detects deuterium-deuterium neutrons through the proton produced in ^{35}Cl(n,p)^{35}S reaction, eliminating the need for a full unfolding process and simplifying the measurement procedure. The CLYC7 scintillator had dimensions of 2.54 cm in diameter

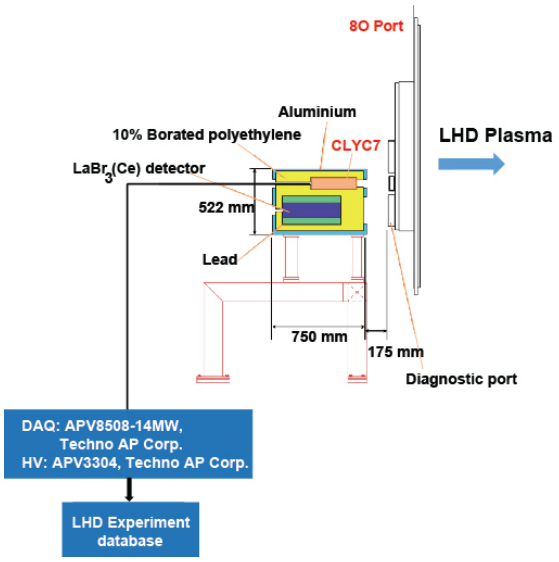

Fig. 4. A schematic cut view of the LHD, featuring the horizontal line-of-sight perpendicular CNES based on CLYC7 operating at the LHD 8-O port.

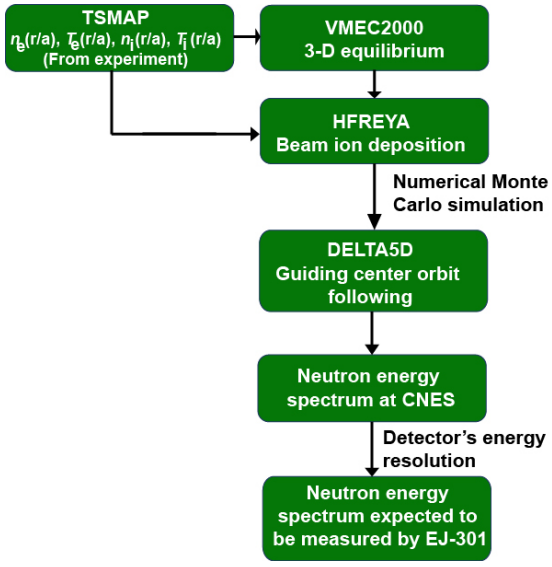

Fig. 5. Diagram illustrating the configuration for simulating the neutron energy spectrum resulting from deuterium-deuterium reaction.

and in height. It was optically coupled with a standard PMT with a diameter of 2.54 cm, specifically model H10580-100-01 of Hamamatsu Photonics K.K. [47]. To supply power to the scintillator, a quad high-voltage power supply model RPH-033 of HAYASHI-REPIC Corp. [48] was employed, providing a high voltage of approximately -1300 V. The process of signal acquisition and data recording was executed using a fast digital data acquisition system, specifically the model APV8508-14MW of Techno AP Corp. [49]. Before the installation in the LHD, the system was characterized over an extensive range of neutron energies in the neutron source facilities [52]. The installation of the perpendicular CNES based on CLYC7 at the 8-O port provides a sight-line horizontally oriented perpendicular with the magnetic field [see Fig. 4]. This arrangement was selected to examine the dynamics of fast ions helically confined in the LHD plasma mid-plane, particularly within the helical ripple. The perpendicular CNES utilizing CLYC7 was housed within a neutron shielding box constructed from 10% borated polyethylene, alongside $LaBr_3$(Ce) and plastic scintillators [53], [54]. The signal was conveyed through a 1 Gbps Ethernet connection and archived in the LHD experiment database. Despite not requiring the unfolding process, the CLYC7 scintillator generates a signal with a relatively long decay time, typically in the order of microseconds. This characteristic restricts its operation to a relatively low S_n region, with a maximum capability of 1.5×10^{13} n/s [38].

IV. Numerical Simulation

To underscore the precision and dependability of the investigation into the dynamics of fast ions helically confined during P-NB heating in the LHD using perpendicular CNESs, the DELTA5D five-dimensional orbit-following code [55] was employed. This calculation was employed to compute the anticipated neutron energy spectrum arising from deuterium-deuterium reaction as observed by perpendicular CNESs. The configuration employed to capture the neutron energy spectrum arising from deuterium-deuterium reactions in this study is depicted in Fig. 4. In the simulations, plasma density and plasma temperature profiles were derived from the TSMAP code, a real-time magnetic coordinate mapping system [56], utilizing experimental plasma data. These profiles were subsequently employed in the VMEC2000 code [57] to reconstruct the three-dimensional equilibrium and in the HFREYA code [58], [59] to ascertain the profiles of the birth position and energy of fast ion resulting from P-NB heating, considering the specific P-NB configuration. Using DELTA5D code, the trajectories of fast ions from P-NB heating were computed in Boozer coordinates. In this analysis, the trajectories of a collective of 10^5 ions are examined. Each ion was followed within 1 s. The fast ions's energy distribution was assessed in both Boozer and Cartesian coordinates. Given the sight-line geometry configuration of the perpendicular CNES, the integrated energy distribution of fast ions along the line was calculated. To model the observed neutron energy spectrum originating from deuterium-deuterium reactions, as detected by the perpendicular CNES, a Monte Carlo numerical simulation was employed. This simulation incorporated parameters such as the energy distribution of fast ion, the Larmor phase of fast ion, and the energy resolution of the detector [44], [45], [52]

V. Results and Discussions

A. Neutron spectroscopy in the P-NB heated plasma

To investigate the confinement of helically-trapped fast ions generated through P-NB heating, we conducted deuterium-deuterium neutron spectroscopy using perpendicular CNESs. Fig. 6 illustrates the temporal evolution of LHD deuterium plasma discharge #183208. To create plasmas with relatively low electron temperatures, thus maintaining a low S_n, we set the toroidal magnetic field strength (B_T) to 1 T, in a clockwise orientation as observed from top-view perspective. The position of the magnetic axis in the vacuum (R_{ax_vac})

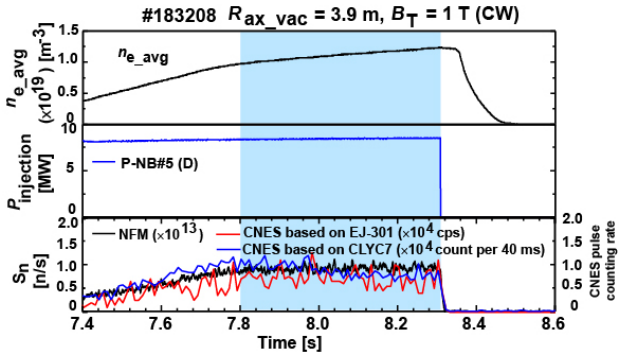

Fig. 6. Plasma discharge #183208 is illustrated in the figure. The top panel shows the line-averaged electron density, the middle panel represents the injection of P-NB#5, and the lower panel exhibits the S_n measured by the neutron flux monitor (NFM), alongside the pulse counting rates recorded by both the perpendicular CNES based on EJ-301 and the perpendicular CNES based on CLYC7. The time interval shaded in blue, spanning from 7.8 to 8.3 s, was chosen for deuterium-deuterium neutron spectroscopy.

was consistently held at 3.9 m. The time interval from 7.8 to 8.3 s, during which plasma was heated by P-NB#5, was chosen for deuterium-deuterium neutron spectroscopy. Note that P-NB#5 delivered fast ion with energy of approximately 70 keV at a power level of about 7.5 MeV. To ensure on statistical measurements, data on deuterium-deuterium neutron emissions during P-NB heating were accumulated from plasma discharges #183193 to #183220, where the plasma configurations were similar. These measurements were conducted using both perpendicular CNES based on EJ-301 and perpendicular CNES based on CLYC7.

During the measurement, the perpendicular CNES based on EJ-301 responded to both neutrons and γ-rays, as clearly illustrated in Fig. 7a. When the incident energy of neutrons and γ-rays are equal, the signal induced by neutrons typically displays a more prolonged decay time in comparison to the signal induced by γ-rays. Therefore, the charge comparison method was utilized to generate the PSD plot [see Fig. 7b], enabling the discrimination between neutron and γ-ray signals and facilitating deuterium-deuterium neutron measurements to investigate the dynamics of helically-trapped beam ions in the LHD. The neutron signal identified in the PSD range from 0.27 to 0.44. However, neutron detection in perpendicular CNES based on EJ-301 relies on neutron-proton elastic scattering. Only recoiled protons with energies covering a range from zero to the incoming neutron energy, vary with the scattering angle, can be detected by the perpendicular CNES based on EJ-301. Fig. 7c displays the integrated charge (Q_{total}) histogram, which was proportional to the histogram of recoil proton energy, acquired during the selected time span from 7.8 to 8.3 s. Hence, an unfolding process is essential to derive the neutron energy spectrum. Employing a suitable unfolding technique, specifically the derivative unfolding method in Eq. 2, we obtained the neutron energy spectrum from the histogram of recoil proton energy, as depicted in Fig. 7d. The neutron energy spectrum arising from deuterium-deuterium reactions during P-NB heating displays a double-humped profile with peaks around 2.30 MeV and 2.74 MeV.

Additionally, neutron spectroscopy for deuterium-deuterium

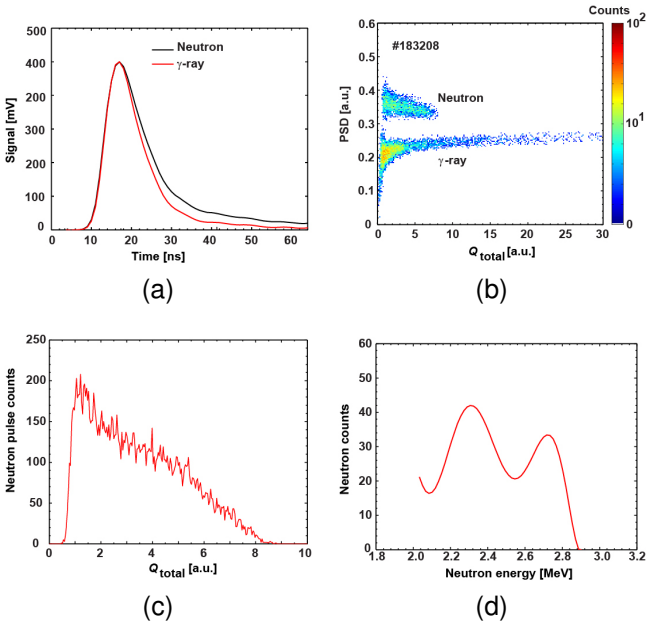

Fig. 7. (a) Standard signals induced by neutrons and γ-rays measured using the perpendicular CNES based on EJ-301. (b) Two-dimensional plot of PSD derived from LHD deuterium plasma discharge #183208. (c) Histogram of Q_{total}. (d) Unfolded neutron energy spectrum resulting from deuterium-deuterium reaction during P-NB heating measured by a perpendicular CNES based on EJ-301 during the selected time interval.

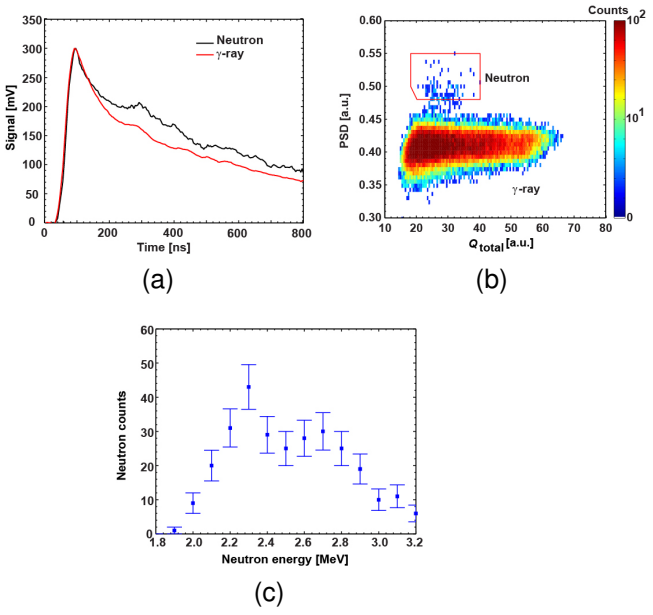

Fig. 8. (a) Standard signals induced by neutrons and γ-rays measured using the perpendicular CNES based on CLYC7. (b) Two-dimensional plot of PSD obtained by accumulating data from plasma discharges between #183193 and #183220. (c) Neutron energy spectrum resulting from deuterium-deuterium reactions during P-NB heating measured using the perpendicular CNES based on CLYC7.

reactions in the P-NB#5 heated plasma was achieved using the perpendicular CNES based on CLYC7. The data were accumulated during the plasma discharges between #183193 and #183220. Similar to the perpendicular CNES based on EJ-301, the perpendicular CNES based on CLYC7 can detect

both neutrons and γ-rays. Fig. 8a clearly shows that when the incident energy of neutrons and γ-rays is equivalent, the signal induced by neutrons typically displays a more prolonged decay time in comparison to the signal induced by γ-rays. Therefore, the method of charge comparison was utilized to create the PSD plot [see Fig. 8b], allowing for the discrimination between neutron and γ-ray signals and enabling deuterium-deuterium neutron measurements to study the dynamics of beam ions helically confined in the LHD. Unlike the perpendicular CNES based on EJ-301, the perpendicular CNES based on CLYC7 detects deuterium-deuterium neutrons through the ^{35}Cl(n,p)^{35}S reactions, eliminating the need for an unfolding method. The deuterium-deuterium neutron spectroscopy in P-NB heated plasma was achieved by the perpendicular CNES based on CLYC7. The resulting spectrum exhibits a double-humped profile featuring peaks around 2.30 MeV and 2.74 MeV as shown in Fig. 8c.

Deuterium-deuterium neutron energy spectra characterized by a double-humped profile were successfully obtained by both perpendicular CNES based on EJ-301 and perpendicular CNES based on CLYC7 in P-NB heated plasma. The presence of two peaks might be indicative of the Larmor motion of fast ions confined within the helical ripple of the LHD. To confirm the experimental findings through comparison with the calculations, the neutron spectrum resulting from deuterium-deuterium reaction was computed utilizing the DELTA5D five-dimensional orbit-following code as described in Sec. IV. Fig. 9a illustrates the fast ion energy distribution from P-NB#5 heating in LHD deuterium plasma discharge #183208 at the time equal to 8.0 s, integrated over the sight-line of the perpendicular CNES. In the LHD, P-NB injection provides a full energy component of about 70 keV, along with energy components at one-half and one-third simultaneously, due to the production of hydrogen molecules within an ion source. Fig. 9b depicts the line-integrated neutron energy spectrum from deuterium-deuterium reaction anticipated at the perpendicular CNES position. This calculation is based on the distribution of fast ion energy, taking into account the Larmor phase. Considering the energy resolution of the detector [45], we calculate the anticipated neutron energy spectrum resulting from deuterium-deuterium reactions to be measured by the perpendicular CNES, as shown by the dashed line spectrum in Fig. 10. The results demonstrate good agreement between calculation and observation of neutron energy spectra from deuterium-deuterium reactions during P-NB heating plasma by both perpendicular CNES based on EJ-301 and perpendicular CNES based on CLYC7 [see Fig. 10]. This agreement underscores the precision and dependability of employing perpendicular CNESs to investigate the dynamics of fast ions helically confined in the LHD.

B. Deuterium-deuterium neutron energy spectrum in plasma heated by P-NB with the superimposition of ICRF waves

With the ICRF wave superimposed on P-NB heating, the fast ion was accelerated, providing high-energy ions up to a few MeV. A feasibility study for measuring the fast ion energy distribution up to 1 MeV shows that the neutron

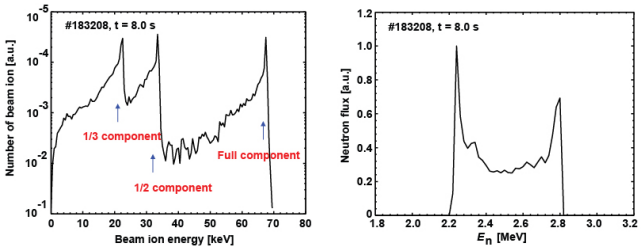

Fig. 9. (a) Fast ion energy distribution integrated over perpendicular CNES line-of-sight. (b) Neutron energy spectrum resulting from deuterium-deuterium reaction at perpendicular CNES position without taking into account the detector energy resolution.

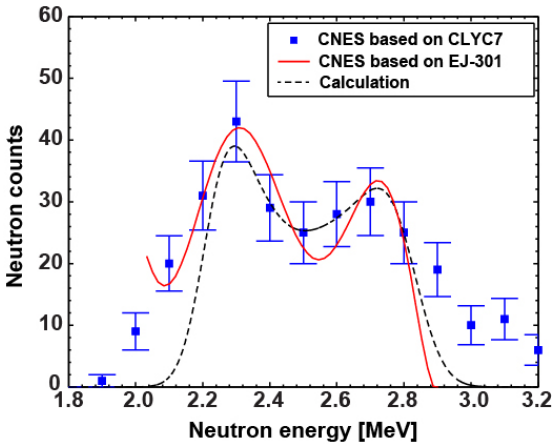

Fig. 10. Neutron energy spectrum from deuterium-deuterium reactions during P-NB heating characterized by a double-humped profile obtained by perpendicular CNES based on EJ-301, by perpendicular CNES based CLYC7, and by calculation.

energy spectrum arising from deuterium-deuterium reaction anticipated to be acquired by the perpendicular CNES has peak locations that become broader with higher fast ion energy [45].

In this study, deuterium-deuterium neutron spectrometry was conducted in plasma discharges #183247, where the plasma was heated by the P-NB#4 and P-NB#5 [see Fig. 11a], and in plasma discharges #183241, where the plasma was heated simultaneously by P-NB#4, P-NB#5, and ICRF waves [see Fig. 11b]. The measurements were performed using the perpendicular CNES based on EJ-301. In the experiment, we set B_T to 2.75 T, in a clockwise orientation as observed from top-view perspective. The R_{ax_vac} was consistently held at 3.6 m. With this configuration, high-performance plasma experiments were conducted. The time span from 3.8 to 5.2 s was selected for deuterium-deuterium neutron spectroscopy. The result shows that the perpendicular CNES provides an effective diagnostic tool for studying fast ion acceleration by ICRF waves. A double-humped profile neutron spectra with peaks at approximately 2.32 MeV and 2.64 MeV were obtained in plasma discharge #183247, where the plasma was heated by the P-NBs. It was observed that the peak becomes broader, especially at the upper-shifted neutron energy due to the ICRF wave heating, as expected [see Fig. 12].

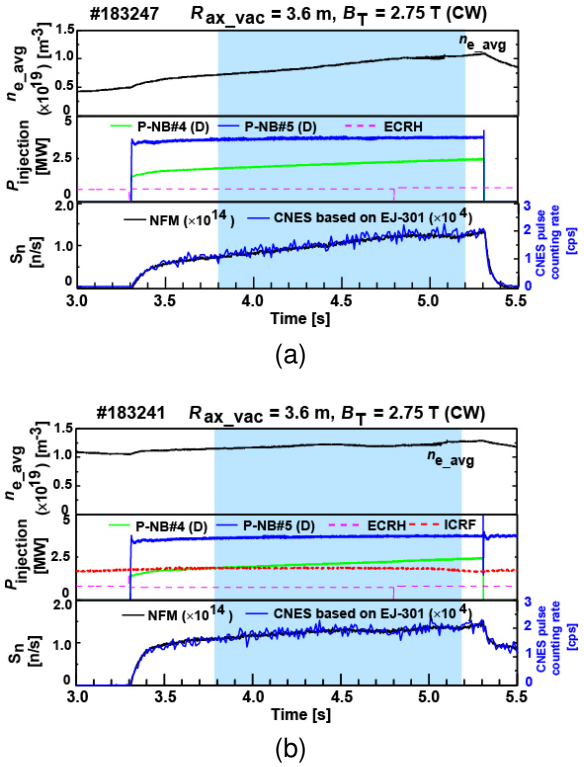

Fig. 11. Plasma discharge (a) #183247 and (b) #183241 were illustrated in the figure. The top panel shows the line-averaged electron density, the middle panel represents the injection of P-NB#4, P-NB#5, and ICRF wave, and the bottom panel displays the S_n measured by NFM, along with the pulse counting rates measured by the perpendicular CNES based on EJ-301. The time interval shaded in blue, spanning from 3.8 to 5.2 s, was chosen for deuterium-deuterium neutron spectroscopy.

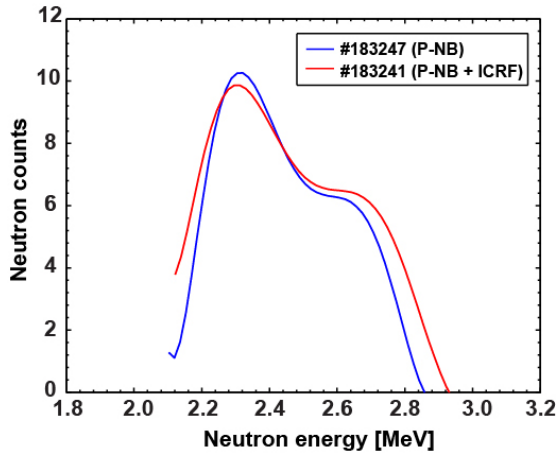

Fig. 12. Neutron energy spectrum from deuterium-deuterium reactions in plasma discharge #183208 heated by P-NB, and in plasma discharge #183241 with ICRF wave superimposed on P-NB heating, measured using the perpendicular CNES based on EJ-301.

VI. Summary

The confinement of fast ions trapped helically generated by perpendicular injection P-NB, which reflected in the deuterium-deuterium neutron energy, was successfully observed using both perpendicular CNES based on EJ-301 and perpendicular CNES based on CLYC7. The neutron spectrum derived from deuterium-deuterium reaction exhibited a double-humped profile corresponded to the Larmor motion of helically-trapped fast ions generated from P-NB heating. To validate the experimental findings pertaining to the dynamics of fast ions helically confined in the LHD, simulations were performed using the DELTA5D code. These simulations considered Larmor motion effects and accounted for the energy resolution of the detector. The agreement between the experimental and simulated neutron energy from deuterium-deuterium reaction underscores the accuracy and ability of use perpendicular CNES to measure the confinement of helically-trapped fast ions generated through P-NB heating in the LHD. The perpendicular CNES based on EJ-301 demonstrated the capability to observe the neutron energy spectrum resulting from deuterium-deuterium reaction in ICRF waves combined with P-NB heated plasma. The results indicated that the peak broadened due to the fast ion acceleration process driven by ICRF waves.

References

[1] A. Fasoli, C. Gormenzano, H. Berk, B. Breizman, S. Briguglio, D. Darrow, N. Gorelenkov, W. Heidbrink, A. Jaun, S. Konovalov, R. Nazikian, J.-M. Noterdaeme, S. Sharapov, K. Shinohara, D. Testa, K. Tobita, Y. Todo, G. Vlad, and F. Zonca, "Chapter 5: Physics of energetic ions," *Nuclear Fusion*, vol. 47, no. 6, p. S264, jun 2007.

[2] W. W. Heidbrink, "Basic physics of Alfvén instabilities driven by energetic particles in toroidally confined plasmasa)," *Physics of Plasmas*, vol. 15, no. 5, p. 055501, 02 2008.

[3] D. Moseev, M. Salewski, M. Garcia-Munoz, B. Geiger, and M. Nocente, "Recent progress in fast-ion diagnostics for magnetically confined plasmas," *Reviews of Modern Plasma Physics*, vol. 2, p. 7, 2018.

[4] W. W. Heidbrink, Y. Luo, K. H. Burrell, R. W. Harvey, R. I. Pinsker, and E. Ruskov, "Measurements of fast-ion acceleration at cyclotron harmonics using balmer-alpha spectroscopy," *Plasma Physics and Controlled Fusion*, vol. 49, no. 9, p. 1457, aug 2007. [Online]. Available: https://dx.doi.org/10.1088/0741-3335/49/9/008

[5] W. W. Heidbrink, "Fast-ion D measurements of the fast-ion distribution (invited)a)," *Review of Scientific Instruments*, vol. 81, no. 10, 10 2010, 10D727.

[6] S. S. Medley, A. J. H. Donné, R. Kaita, A. I. Kislyakov, M. P. Petrov, and A. L. Roquemore, "Invited Review Article: Contemporary instrumentation and application of charge exchange neutral particle diagnostics in magnetic fusion energy experiments," *Review of Scientific Instruments*, vol. 79, no. 1, 01 2008, 011101.

[7] D. Liu, W. W. Heidbrink, K. Tritz, E. D. Fredrickson, G. Z. Hao, and Y. B. Zhu, "Compact and multi-view solid state neutral particle analyzer arrays on National Spherical Torus Experiment-Upgrade," *Review of Scientific Instruments*, vol. 87, no. 11, p. 11D803, 07 2016. [Online]. Available: https://doi.org/10.1063/1.4959798

[8] O. Jarvis, "Neutron measurement techniques for tokamak plasmas," *Plasma physics and controlled fusion*, vol. 36, no. 2, p. 209, 1994.

[9] ——, "Neutron spectrometry at jet (1983–1999)," *Nuclear Instruments and Methods in Physics Research Section A: Accelerators, Spectrometers, Detectors and Associated Equipment*, vol. 476, no. 1, pp. 474–484, 2002, int. Workshop on Neutron Field Spectrometry in Science, Technolog y and Radiation Protection.

[10] G. Ericsson, "Advanced neutron spectroscopy in fusion research," *Journal of Fusion Energy*, vol. 38, no. 3, pp. 330–355, 2019.

[11] M. Tardocchi, M. Nocente, and G. Gorini, "Diagnosis of physical parameters of fast particles in high power fusion plasmas with high resolution neutron and gamma-ray spectroscopy," *Plasma Physics and Controlled Fusion*, vol. 55, no. 7, p. 074014, jun 2013.

[12] G. Ericsson, L. Ballabio, S. Conroy, J. Frenje, H. Henriksson, A. Hjalmarsson, J. Källne, and M. Tardocchi, "Neutron emission spectroscopy at JET—Results from the magnetic proton recoil spectrometer (invited)," *Review of Scientific Instruments*, vol. 72, no. 1, pp. 759–766, 01 2001.

[13] M. Gatu Johnson, L. Giacomelli, A. Hjalmarsson, J. Källne, M. Weiszflog, E. Andersson Sundén, S. Conroy, G. Ericsson, C. Hellesen, E. Ronchi, H. Sjöstrand, G. Gorini, M. Tardocchi, A. Combo,

N. Cruz, J. Sousa, and S. Popovichev, "The 2.5-mev neutron time-of-flight spectrometer tofor for experiments at jet," *Nuclear Instruments and Methods in Physics Research Section A: Accelerators, Spectrometers, Detectors and Associated Equipment*, vol. 591, no. 2, pp. 417–430, 2008.

[14] A. V. Krasilnikov, J. Kaneko, M. Isobe, F. Maekawa, and T. Nishitani, "Fusion Neutronic Source deuterium–tritium neutron spectrum measurements using natural diamond detectors," *Review of Scientific Instruments*, vol. 68, no. 4, pp. 1720–1724, 04 1997. [Online]. Available: https://doi.org/10.1063/1.1148001

[15] C. Cazzaniga, E. A. Sundén, F. Binda, G. Croci, G. Ericsson, L. Giacomelli, G. Gorini, E. Griesmayer, G. Grosso, G. Kaveney, M. Nocente, E. P. Cippo, M. Rebai, B. Syme, M. Tardocchi, and J.-E. Contributors, "Single crystal diamond detector measurements of deuterium-deuterium and deuterium-tritium neutrons in Joint European Torus fusion plasmas," *Review of Scientific Instruments*, vol. 85, no. 4, 04 2014, 043506.

[16] G. Tardini, F. Gagnon-Moisan, and A. Zimbal, "Characterisation of a BC501A compact neutron spectrometer for fusion research," *Review of Scientific Instruments*, vol. 87, no. 10, 10 2016, 103504.

[17] A. Zimbal, L. Bertalot, H. Schuhmacher, M. Reginatto, H. Klein, and A. Murari, "High resolution neutron spectrometry with liquid scintillation detectors for fusion applications," *PoS*, p. 035, 2006.

[18] K. Toi, K. Ogawa, M. Isobe, M. Osakabe, D. A. Spong, and Y. Todo, "Energetic-ion-driven global instabilities in stellarator/helical plasmas and comparison with tokamak plasmas," *Plasma Physics and Controlled Fusion*, vol. 53, no. 2, p. 024008, jan 2011. [Online]. Available: https://dx.doi.org/10.1088/0741-3335/53/2/024008

[19] M. Osakabe, M. Isobe, S. Murakami, S. Kobayashi, K. Saito, R. Kumazawa, T. Mutoh, T. Ozaki, M. Nishiura, E. Veshchev, T. Seki, Y. Takeiri, O. Kaneko, K. Nagaoka, T. Tokuzawa, K. Ogawa, K. Toi, S. Yamamoto, M. Sasao, T. Watanabe, and L. E. Group, "Fast-ion confinement studies on lhd," *Fusion Science and Technology*, vol. 58, no. 1, pp. 131–140, 2010.

[20] M. Isobe, M. Osakabe, T. Ozaki, M. Nishiura, P. V. Goncharov, E. Veshchev, K. Ogawa, K. Nagaoka, K. Saito, S. Murakami, T. Saida, M. Sasao, K. Toi, and L. E. Group, "Fast-particle diagnostics on lhd," *Fusion Science and Technology*, vol. 58, no. 1, pp. 426–435, 2010.

[21] T. Saida, M. Sasao, M. Isobe, A. Krasilnikov, R. Kumazawa, T. Mutoh, T. Watari, T. Seki, K. Saito, S. Murakami, K. Matsuoka, and L. E. Group, "Study of ripple-trapped proton behaviour in lhd by two line-of-sight measurements of fast neutrals," *Nuclear Fusion*, vol. 44, no. 4, p. 488, mar 2004.

[22] M. Osakabe, S. Yamamoto, K. Toi, Y. Takeiri, S. Sakakibara, K. Nagaoka, K. Tanaka, K. Narihara, L. E. Group *et al.*, "Experimental observations of enhanced radial transport of energetic particles with alfvén eigenmode on the lhd," *Nuclear fusion*, vol. 46, no. 10, p. S911, 2006.

[23] K. Ogawa, M. Isobe, K. Toi, F. Watanabe, D. A. Spong, A. Shimizu, M. Osakabe, S. Ohdachi, S. Sakakibara, L. E. Group *et al.*, "Observation of energetic-ion losses induced by various mhd instabilities in the large helical device (lhd)," *Nuclear fusion*, vol. 50, no. 8, p. 084005, 2010.

[24] K. Ogawa, M. Isobe, K. Toi, D. A. Spong, M. Osakabe, and L. E. Group, "Magnetic configuration effects on tae-induced losses and a comparison with the orbit-following model in the large helical device," *Nuclear Fusion*, vol. 52, no. 9, p. 094013, sep 2012. [Online]. Available: https://dx.doi.org/10.1088/0029-5515/52/9/094013

[25] R. Seki, Y. Todo, Y. Suzuki, D. Spong, K. Ogawa, M. Isobe, and M. Osakabe, "Comprehensive magnetohydrodynamic hybrid simulations of alfvén eigenmode bursts and fast-ion losses in the large helical device," *Nuclear Fusion*, vol. 59, no. 9, p. 096018, jul 2019. [Online]. Available: https://dx.doi.org/10.1088/1741-4326/ab266e

[26] M. Osakabe, Y. Takeiri, T. Morisaki, G. Motojima, K. Ogawa, M. Isobe, M. Tanaka, S. Murakami, A. Shimizu, K. Nagaoka, H. Takahashi, K. Nagasaki, H. Takahashi, T. Fujita, Y. Oya, M. Sakamoto, Y. Ueda, T. Akiyama, H. Kasahara, S. Sakakibara, R. Sakamoto, M. Tokitani, H. Yamada, M. Yokoyama, Y. Yoshimura, and L. E. Group, "Current status of large helical device and its prospect for deuterium experiment," *Fusion Science and Technology*, vol. 72, no. 3, pp. 199–210, 2017.

[27] M. Isobe, K. Ogawa, T. Nishitani, N. Pu, H. Kawase, R. Seki, H. Nuga, E. Takada, S. Murakami, Y. Suzuki *et al.*, "Fusion neutron production with deuterium neutral beam injection and enhancement of energetic-particle physics study in the large helical device," *Nuclear Fusion*, vol. 58, no. 8, p. 082004, 2018.

[28] M. Isobe, K. Ogawa, T. Nishitani, H. Miyake, T. Kobuchi, N. Pu, H. Kawase, E. Takada, T. Tanaka, S. Li *et al.*, "Neutron diagnostics in the large helical device," *IEEE Transactions on Plasma Science*, vol. 46, no. 6, pp. 2050–2058, 2018.

[29] K. Ogawa, M. Isobe, T. Nishitani, S. Murakami, R. Seki, H. Nuga, S. Kamio, Y. Fujiwara, H. Yamaguchi, Y. Saito *et al.*, "Energetic ion confinement studies using comprehensive neutron diagnostics in the large helical device," *Nuclear Fusion*, vol. 59, no. 7, p. 076017, 2019.

[30] K. Ogawa, M. Isobe, and M. Osakabe, "Progress on integrated neutron diagnostics for deuterium plasma experiments and energetic particle confinement studies in the large helical device during the campaigns from fy2017 to fy2019," *Plasma and Fusion Research*, vol. 16, pp. 1 102 023–1 102 023, 2021.

[31] S. Sangaroon, K. Ogawa, M. Isobe, M. I. Kobayashi, Y. Fujiwara, S. Kamio, R. Seki, H. Nuga, H. Yamaguchi, and M. Osakabe, "Performance of the newly installed vertical neutron cameras for low neutron yield discharges in the large helical device," *Review of Scientific Instruments*, vol. 91, no. 8, p. 083505, 2020.

[32] S. Sangaroon, K. Ogawa, M. Isobe, Y. Fujiwara, H. Yamaguchi, S. Kamio, R. Seki, H. Nuga, M. I. Kobayashi, and M. Osakabe, "Characterization of the new vertical neutron camera designed for the low neutron emission rate plasma in large helical device," *Plasma and Fusion Research*, vol. 16, pp. 1 402 039–1 402 039, 2021.

[33] K. Ogawa, M. Isobe, H. Kawase, T. Nishitani, R. Seki, M. Osakabe, L. E. Group *et al.*, "Observation of enhanced radial transport of energetic ion due to energetic particle mode destabilized by helically-trapped energetic ion in the large helical device," *Nuclear Fusion*, vol. 58, no. 4, p. 044001, 2018.

[34] K. Ogawa, M. Isobe, H. Kawase, T. Nishitani, R. Seki, M. Osakabe, and L. E. Group, "Effect of the helically-trapped energetic-ion-driven resistive interchange modes on energetic ion confinement in the large helical device," *Plasma Physics and Controlled Fusion*, vol. 60, no. 4, p. 044005, feb 2018. [Online]. Available: https://dx.doi.org/10.1088/1361-6587/aaab1f

[35] K. Ogawa, M. Isobe, S. Sugiyama, H. Matsuura, D. A. Spong, H. Nuga, R. Seki, S. Kamio, Y. Fujiwara, H. Yamaguchi *et al.*, "Energetic particle transport and loss induced by helically-trapped energetic-ion-driven resistive interchange modes in the large helical device," *Nuclear Fusion*, vol. 60, no. 11, p. 112011, 2020.

[36] S. Sangaroon, K. Ogawa, M. Isobe, M. I. Kobayashi, S. Conroy, Y. Zhang, T. Fan, and M. Osakabe, "Neutron and gamma-ray transport calculations in support of the design of the radiation shielding for the tofed neutron spectrometer at lhd," *Fusion Engineering and Design*, vol. 166, p. 112296, 2021.

[37] Y. Zhang, L. Ge, Z. Hu, J. Sun, X. Li, K. Ogawa, M. Isobe, S. Sangaroon, L. Liao, D. Yang *et al.*, "Design and optimization of an advanced time-of-flight neutron spectrometer for deuterium plasmas of the large helical device," *Review of Scientific Instruments*, vol. 92, no. 5, p. 053547, 2021.

[38] S. Sangaroon, K. Ogawa, M. Isobe, M. Kobayashi, Y. Fujiwara, S. Kamio, H. Yamaguchi, R. Seki, H. Nuga, S. Toyama *et al.*, "Neutron energy spectrum measurement using clyc7-based compact neutron emission spectrometer in the large helical device," *Journal of Instrumentation*, vol. 16, no. 12, p. C12025, 2021.

[39] S. Sangaroon, K. Ogawa, M. Isobe, M. Kobayashi, Y. Fujiwara, S. Kamio, H. Yamaguchi, R. Seki, H. Nuga, E. Takada *et al.*, "Observation of significant doppler shift in deuterium-deuterium neutron energy caused by neutral beam injection in the large helical device," *AAPPS Bulletin*, vol. 32, no. 1, p. 5, 2022.

[40] M. Isobe, K. Ogawa, S. Sangaroon, G. Zhong, and T. Fan, "Recent progress of neutron spectrometer development for lhd deuterium plasmas," *Plasma and Fusion Research*, vol. 17, pp. 2 402 008–2 402 008, 2022.

[41] M. Isobe, K. Ogawa, S. Sangaroon, S. Kamio, Y. Fujiwara, and M. Osakabe, "Recent development of neutron and energetic-particle diagnostics for lhd deuterium discharges," *Journal of Instrumentation*, vol. 17, no. 03, p. C03036, 2022.

[42] M. Isobe, D. Funaki, and M. Sasao, "Lorentz alpha orbit calculation in search of position suitable for escaping alpha particle diagnostics in iter," *J. Plasma Fusion Res. SERIES*, vol. 8, p. 330, 2009.

[43] H. Brysk, "Fusion neutron energies and spectra," *Plasma Physics*, vol. 15, no. 7, p. 611, 1973.

[44] S. Sangaroon, K. Ogawa, M. Isobe, L. Liao, M. I. Kobayashi, G. Zhong, S. Toyama, M. Miwa, S. Matsuyama, E. Takada, A. Wisitsorasak, N. Poolyarat, and M. Osakabe, "Characterization of liquid scintillator-based cnes for deuterium–deuterium neutron emission spectroscopy in the lhd," *IEEE Transactions on Instrumentation and Measurement*, vol. 72, pp. 1–10, 2023.

[45] S. Sangaroon, K. Ogawa, and M. Isobe, "Initial operation of perpendicular line-of-sight compact neutron emission spectrometer in the large helical device," *Review of Scientific Instruments*, vol. 93, no. 9, p. 093504, 2022.

[46] Ej301. [Online]. Available: https://eljentechnology.com/products/liquid-scintillators/ej-301-ej-309
[47] Pmt. [Online]. Available: https://www.hamamatsu.com/resources/pdf/etd/High_energy_PMT_TPMZ0003E.pdf
[48] Hv. [Online]. Available: https://www.h-repic.co.jp/pdf/RPH-034.pdf
[49] Apv_adc. [Online]. Available: http://www.techno-ap.com/img/APV8102-14MWPSAGb_e.pdf
[50] D. Slaughter and R. Strout II, "Flyspec: A simple method of unfolding neutron energy spectra measured with ne213 and stilbene spectrometers," *Nuclear Instruments and Methods in Physics Research*, vol. 198, no. 2-3, pp. 349–355, 1982.
[51] V. Verbinski, W. Burrus, T. Love, W. Zobel, N. Hill, and R. Textor, "Calibration of an organic scintillator for neutron spectrometry," *Nuclear Instruments and Methods*, vol. 65, no. 1, pp. 8–25, 1968.
[52] S. Sangaroon, K. Ogawa, M. Isobe, L. Liao, M. I. Kobayashi, S. Toyama, M. Miwa, S. Matsuyama, H. Yamanishi, S. Tamaki, I. Murata, E. Takada, G. Zhong, A. Wisitsorasak, and N. Poolyarat, "Characterization of clyc7 scintillation detector in wide neutron energy range for fusion neutron spectroscopy," *IEEE Transactions on Instrumentation and Measurement*, vol. 72, pp. 1–12, 2023.
[53] K. OGAWA, S. SANGAROON, and M. ISOBE, "Large volume and fast response gamma ray diagnostic in the large helical device," *Plasma and Fusion Research*, vol. 18, pp. 2 402 016–2 402 016, 2023.
[54] K. Ogawa, S. Sangaroon, L. Liao, H. Matsuura, K. Kimura, D. Umezaki, M. Naoi, T. Fukuda, S. Wakisaka, and M. Isobe, "Gamma ray diagnostics for high time resolution measurement in large helical device," *Journal of Instrumentation*, vol. 18, no. 09, p. P09024, sep 2023. [Online]. Available: https://dx.doi.org/10.1088/1748-0221/18/09/P09024
[55] D. A. Spong, "Three-dimensional effects on energetic particle confinement and stability," *Physics of Plasmas*, vol. 18, no. 5, p. 056109, 2011.
[56] C. Suzuki, K. Ida, Y. Suzuki, M. Yoshida, M. Emoto, and M. Yokoyama, "Development and application of real-time magnetic coordinate mapping system in the large helical device," *Plasma Physics and Controlled Fusion*, vol. 55, no. 1, p. 014016, 2012.
[57] S. Hirshman and O. Betancourt, "Preconditioned descent algorithm for rapid calculations of magnetohydrodynamic equilibria," *Journal of Computational Physics*, vol. 96, no. 1, pp. 99–109, 1991.
[58] S. Murakami, N. Nakajima, and M. Okamoto, "Finite β effects on the icrf and nbi heating in the large helical device," *Fusion Technology*, vol. 27, no. 3T, pp. 256–259, 1995.
[59] P. Vincenzi, T. Bolzonella, S. Murakami, M. Osakabe, R. Seki, and M. Yokoyama, "Upgrades and application of fit3d nbi–plasma interaction code in view of lhd deuterium campaigns," *Plasma Physics and Controlled Fusion*, vol. 58, no. 12, p. 125008, 2016.

Siriyaporn Sangaroon was born in Phatthalung, Thailand, in 1980. She received the M.S. degree in nuclear technology from Chulalongkorn University, Bangkok, Thailand, in 2005, and the Ph.D. degree in physics from Uppsala University, Uppsala, Sweden, in 2014. She has been with the Department of Physics, Faculty of Science, Mahasarakham University, Maha Sarakham, Thailand, since 2005. She is currently an Associate Professor at Mahasarakham University, a role she has held since 2018. Her research focuses on neutron measurement in magnetically confined fusion plasmas.

Kunihiro Ogawa was born in Mino, Gifu, Japan, in 1984. He received the M.S. and Ph.D. degrees from the Department of Energy Science and Engineering, Nagoya University, Nagoya, Japan, in 2008 and 2011, respectively. He studied electrical and electronic engineering at Ritsumeikan University, Kyoto, Japan, from 2003 to 2006. He has been with the National Institute for Fusion Science, Toki, Japan, since 2012. He has been an Associate Professor with the National Institute for Fusion Science since 2020. His current research interests include the energetic-ion confinement in magnetically confined fusion plasmas.

Mitsutaka Isobe was born in Nagoya, Aichi, Japan, in 1967. He received the B.S. and M.S. degrees in applied physics from Fukui University, Fukui, Japan, in 1991 and 1993, respectively, and the Ph.D. degree in fusion science from the Graduate University for Advanced Studies, SOKENDAI, Hayama, Japan, in 1996. He had been involved in a compact helical system project from 1997 to 2006 and is currently involved in a large helical device (LHD) project. He has been a Professor with the National Institute for Fusion Science, Toki, Japan, since 2015. His current research interests include the confinement study of energetic ions by means of neutron diagnostics in magnetically confined fusion plasmas.

Longyong Liao photograph and biography not available at the time of publication.

Guoqiang Zhong photograph and biography not available at the time of publication.

Apiwat Wisitsorasak as born in Bangkok, Thailand, in 1986. He received the B.Sc. degree in physics from Mahidol University, Salaya, Thailand, in 2008, and the Ph.D. degrees from the Department of Physics and Astronomy, Rice University, Houston, TX, USA, in 2014. He is currently with the Department of Physics, King Mongkut's University of Technology Thonburi, Bangkok. His research focuses on energetic-ion confinement and plasma transport in magnetically confined fusion plasmas.

Eiji Takada was born in Toyama, Japan, in 1964. He received the B.S., M.S., and Ph.D. degrees in nuclear engineering from The University of Tokyo, Tokyo, Japan, in 1986, 1988, and 1998, respectively. From 1988 to 1994, he was with Mitsubishi Research Institute, Inc., Tokyo, where he was involved in research on global environmental change. From 1994 to 1999, he was with The University of Tokyo, where he was involved in the radiation measurement with optical fibers. Since 2022, he has been with the National Institute of Technology, Hachioji, Japan. He is also involved in the new types of radiation detectors as those with organic semiconductor materials. His current research interests include neutron diagnostics in fusion experimental devices.

Makoto Inami Kobayashi was born in Fujinomiya, Shizuoka, Japan, in 1986. He received the Ph.D. degree in science from Shizuoka University, Shizuoka, Japan, in 2014. He worked in the Shizuoka prefectural government for environmental radiation research from 2014 to 2016. He has been an Assistant Professor with the National Institute for Fusion Science, Toki, Japan, since 2016. His current research interests include tritium and radiation transports in fusion systems.

Nopporn Poolyarat photograph and biography not available at the time of publication.

Sadayoshi Murakami photograph and biography not available at the time of publication.

Ryohsuke Seki photograph and biography not available at the time of publication.

Hideo nuga photograph and biography not available at the time of publication.

Masaki Osakabe photograph and biography not available at the time of publication.